Supporting Information

Coordinated Optical Matching of a Texture Interface Made from Demixing Blended Polymers for High Performance Inverted Perovskite Solar Cells

Cun Yun Xu,[†,‡] Wei Hu,[†,‡] Gang Wang,[†] Lianbin Niu,[§] Ahmed Mourtada Elseman,[†,‖]

Liping Liao,[†] Yanqing Yao,[†] Gaobo Xu,[†] Lie Luo,[†] Debei Liu,[†] Guangdong Zhou,[†]

*Ping Li,[⊥] Qunliang Song, [†,]**

† Institute for Clean Energy and Advanced Materials, School of Materials and Energy, Southwest University, Chongqing Key Laboratory for Advanced Materials and Technologies of Clean Energy, Chongqing 400715, P. R. China.

§College of Physics and Electronics Engineering, Chongqing Normal University, Chongqing 401331, P. R. China.

‖ Electronic & Magnetic Materials Department, Advanced Materials Division, Central Metallurgical Research and Development Institute (CMRDI), Helwan, P.O. Box 87, Cairo 11421, Egypt.

⊥ School of Physics and Electronic Science, Zunyi Normal College, Zunyi 563002, P.R. China.

‡ Cun Yun Xu and Wei Hu contributed equally to this work.

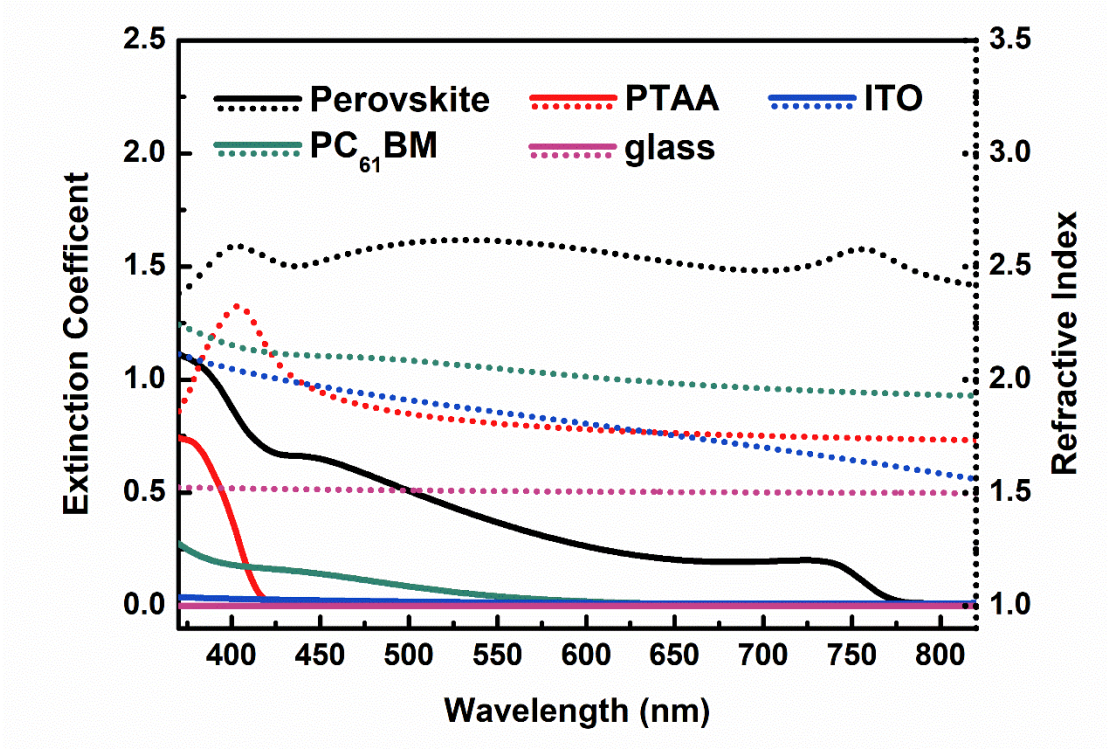

Figure S1. The refractive index (n, dot line), extinction coefficient (k, solid line) values of glass substrate, ITO, PTAA, $PC_{61}BM$ and perovskite.

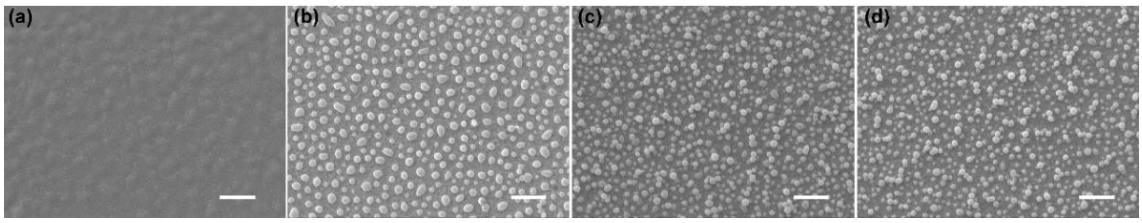

Figure S2. The top view images of final plane and textured PTAA, a) pure PTAA, b) 5:12, c) 5:20 and d) 5:45 PTAA to PS. The texture structure was obtained by washing away PS from the mixed film. The scale bar is 500 nm.

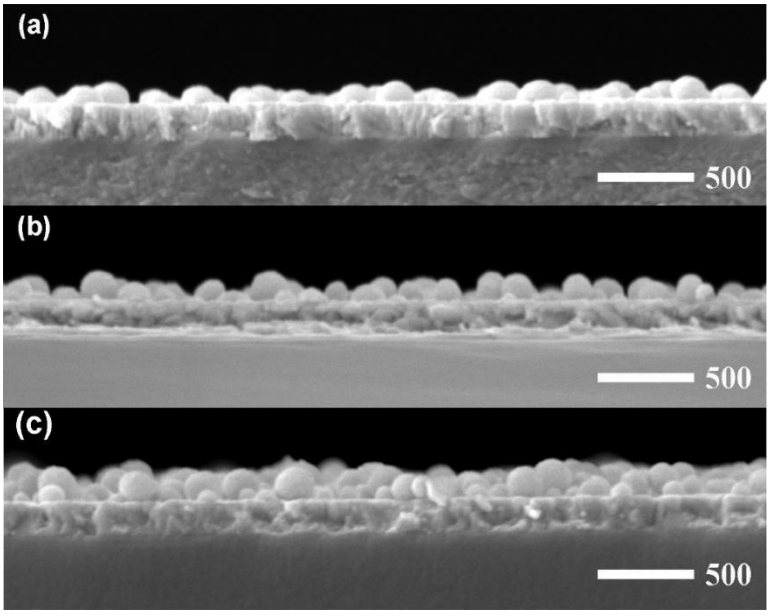

Figure S3. The cross-sectional images of different textured PTAA, by demixing of binary polymer layers. The PTAA to PS mixing ratios were a) 5:12, b) 5:20 and c) 5:45, respectively. The scale bar is 500 nm.

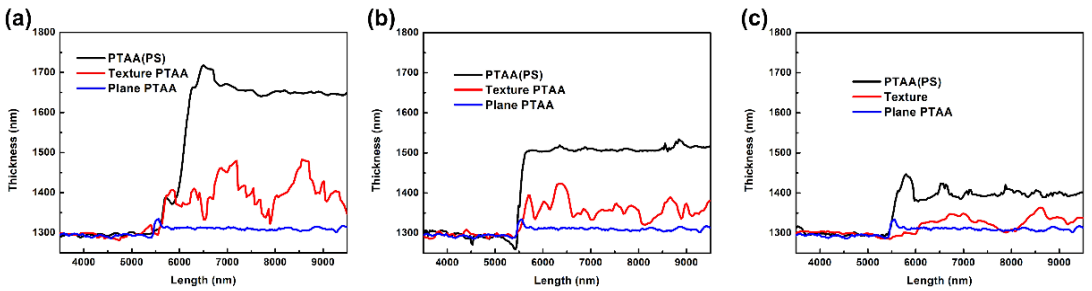

Figure. S4. The thickness of the PTAA/PS mixed layer, textured PTAA layer and plane PTAA layer obtained by using AFM to cross-sectional scan the film after removing half of the layers. The PTAA/PS ratios are 5:45 (a), 5:20 (b) and 5:12 (c) respectively.

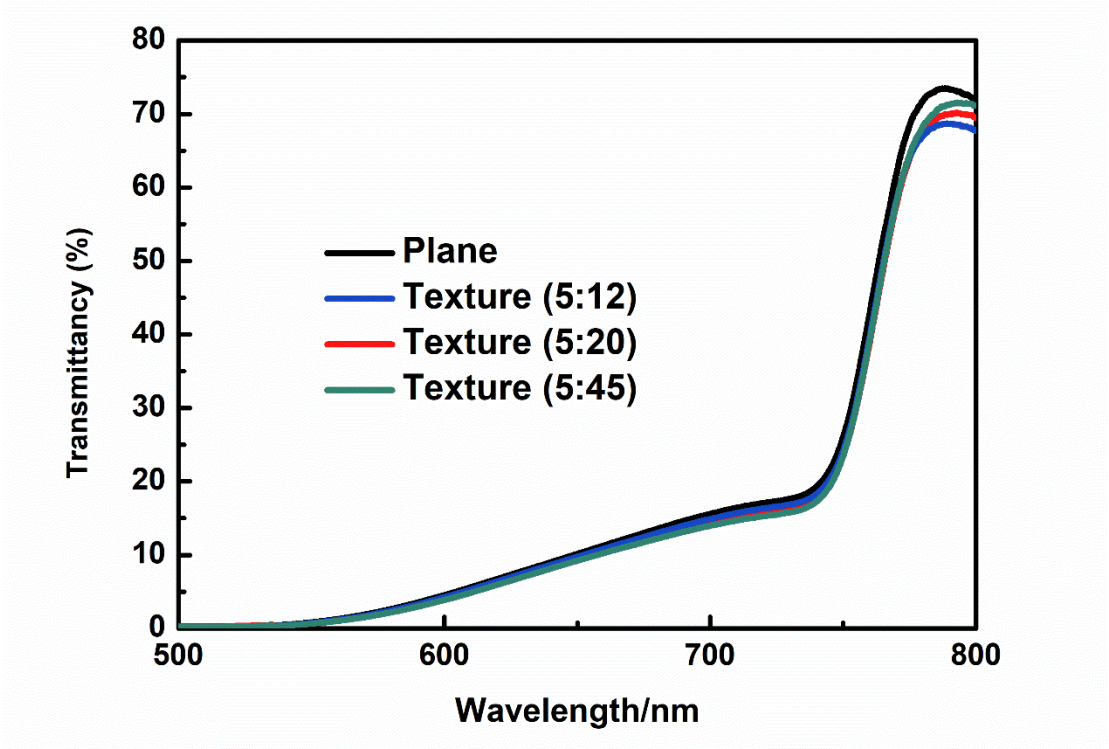

Figure S5. The transmittance of the Glass/ITO/PTAA/Perovskite semi-finished device with plane and different textures.

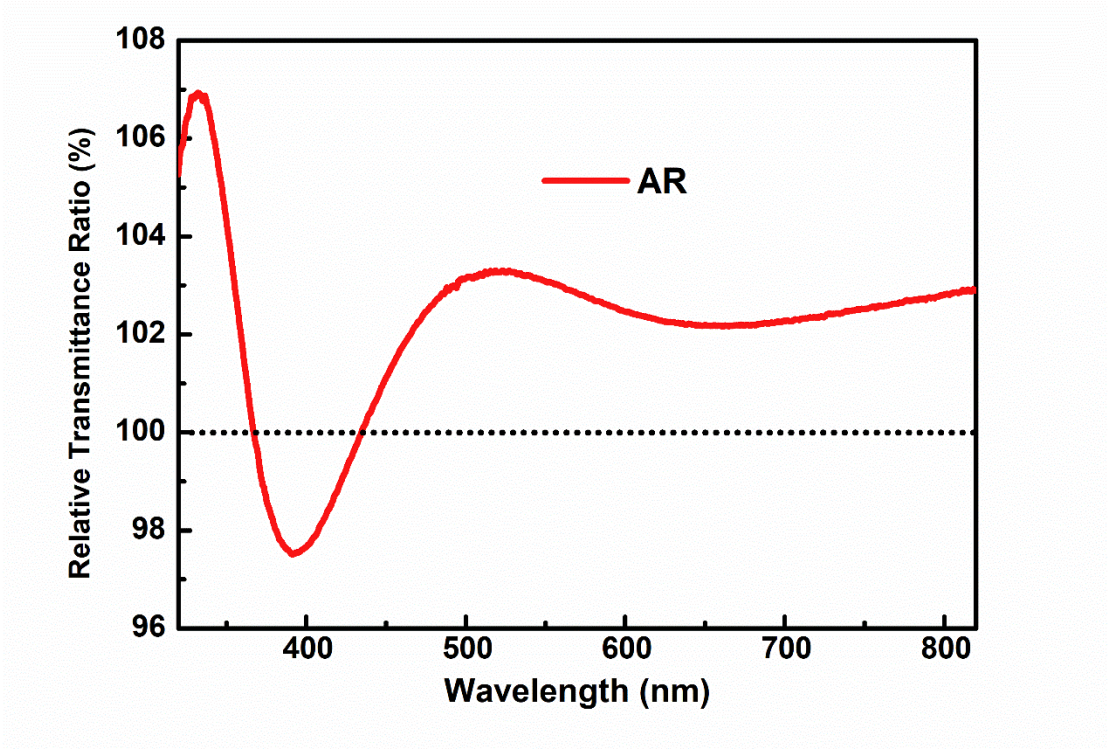

Figure S6. The relative transmittance after coating 125 nm MgF_2 anti-reflection layer. The ratio is achieved by dividing the transmittance after AR coating with the transmittance before AR coating.

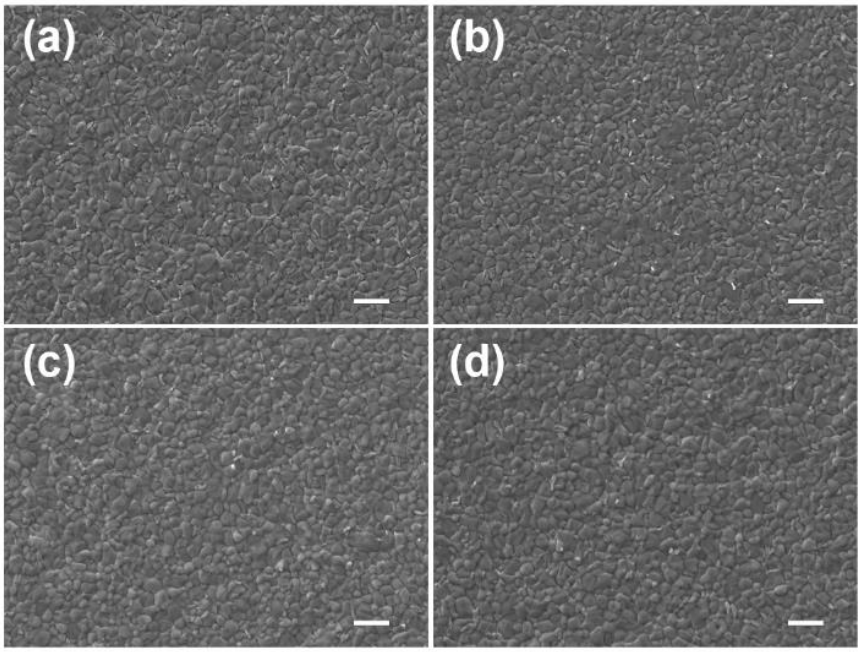

Figure S7. The SEM images of the perovskite layers prepared on different substrates, a) pure PTAA, texture PTAA obtained from b) 5:12, c) 5:20 and d) 5:45 PTAA to PS. The scale bar is 1 μm.

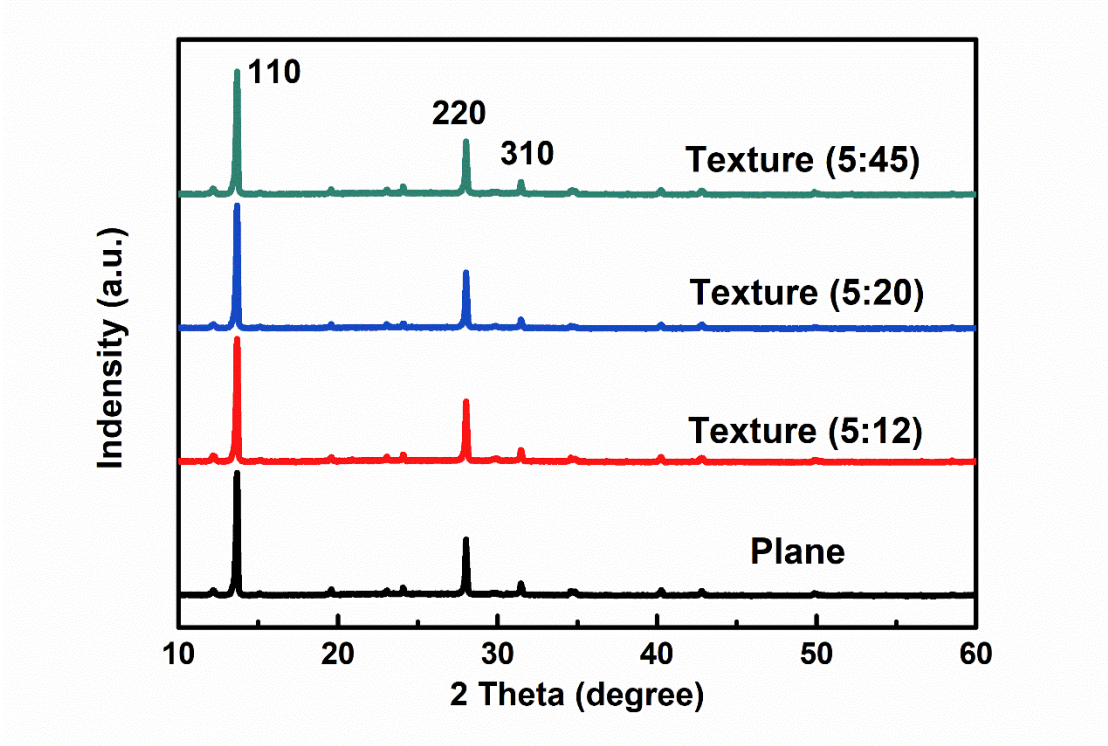

Figure S8. The XRD of the perovskite films prepared on different substrates.

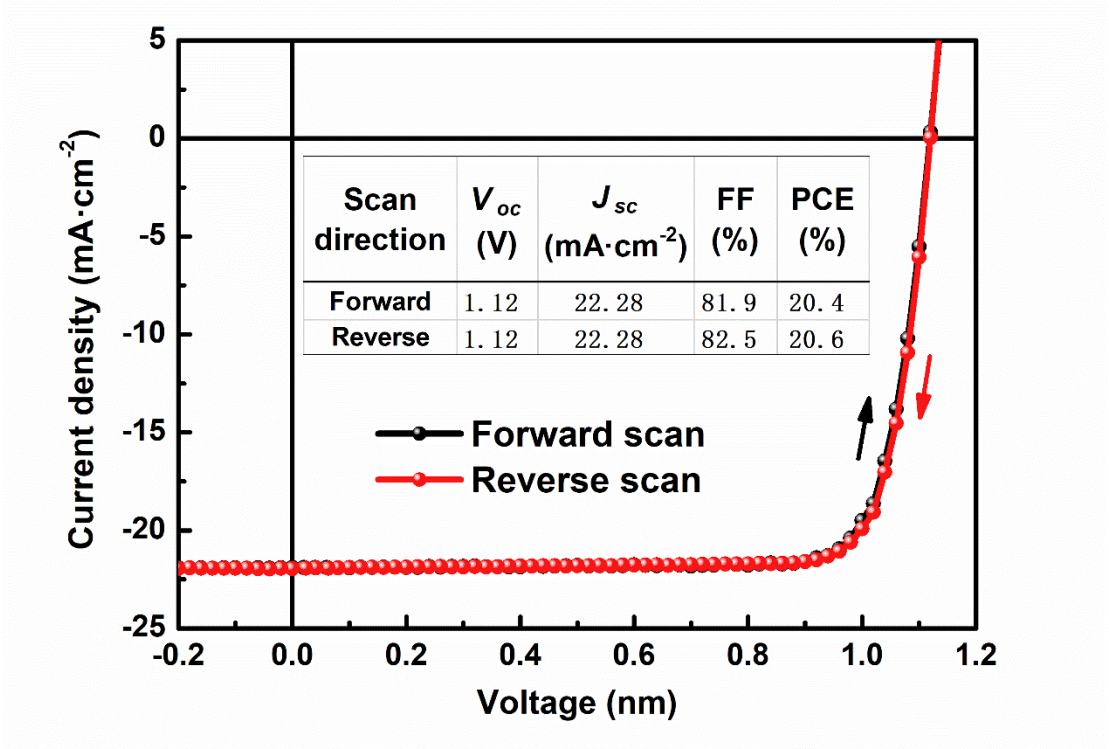

Scan direction	V_{oc} (V)	J_{sc} (mA·cm^{-2})	FF (%)	PCE (%)
Forward	1.12	22.28	81.9	20.4
Reverse	1.12	22.28	82.5	20.6

Figure S9. J-V curves of the texture PTAA solar cell measured under forward and reverse scan.

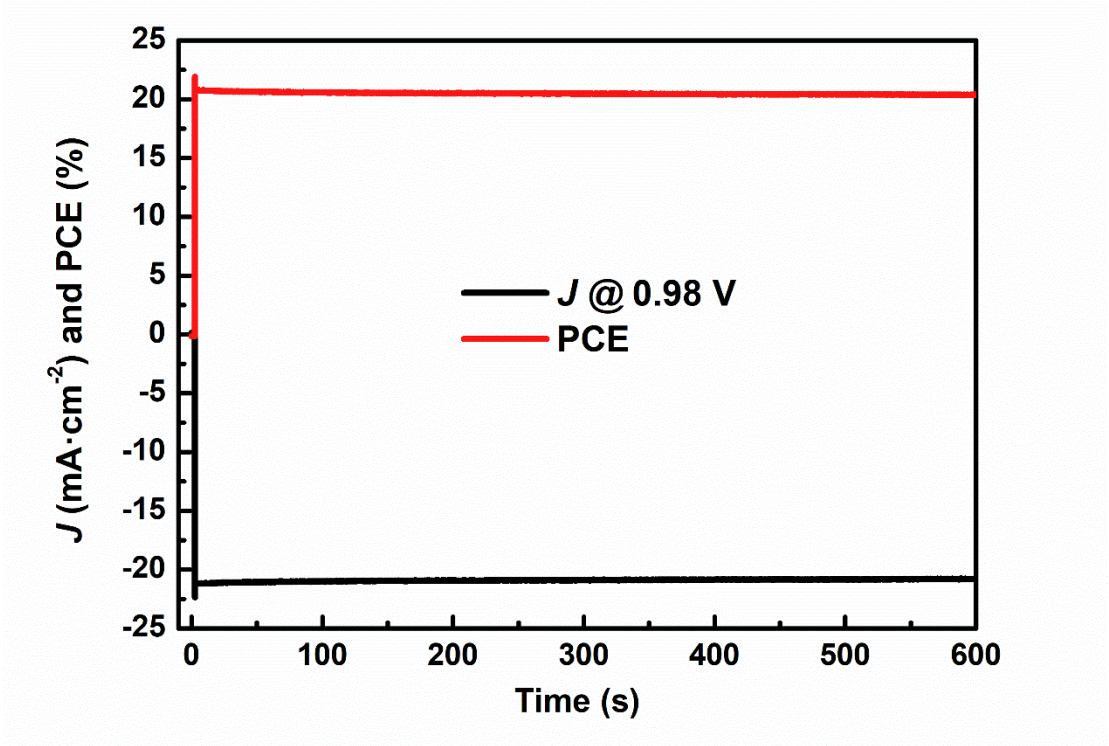

Figure S10. The steady-state output of the current with the optimal power output point (the voltage is about 0.98 V) for 10 minutes and corresponding power conversion efficiency.

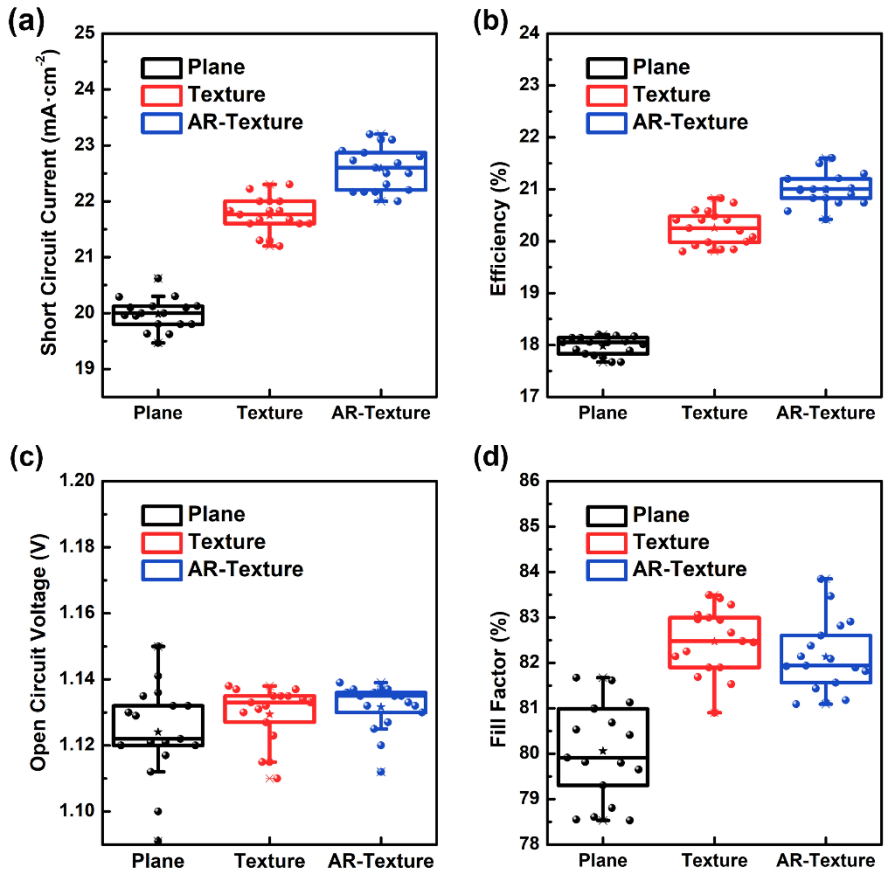

Figure S11. The summary of output characteristics of a) PCE, b) V_{OC}, c) J_{SC} and d) FF from 17 batches of devices.

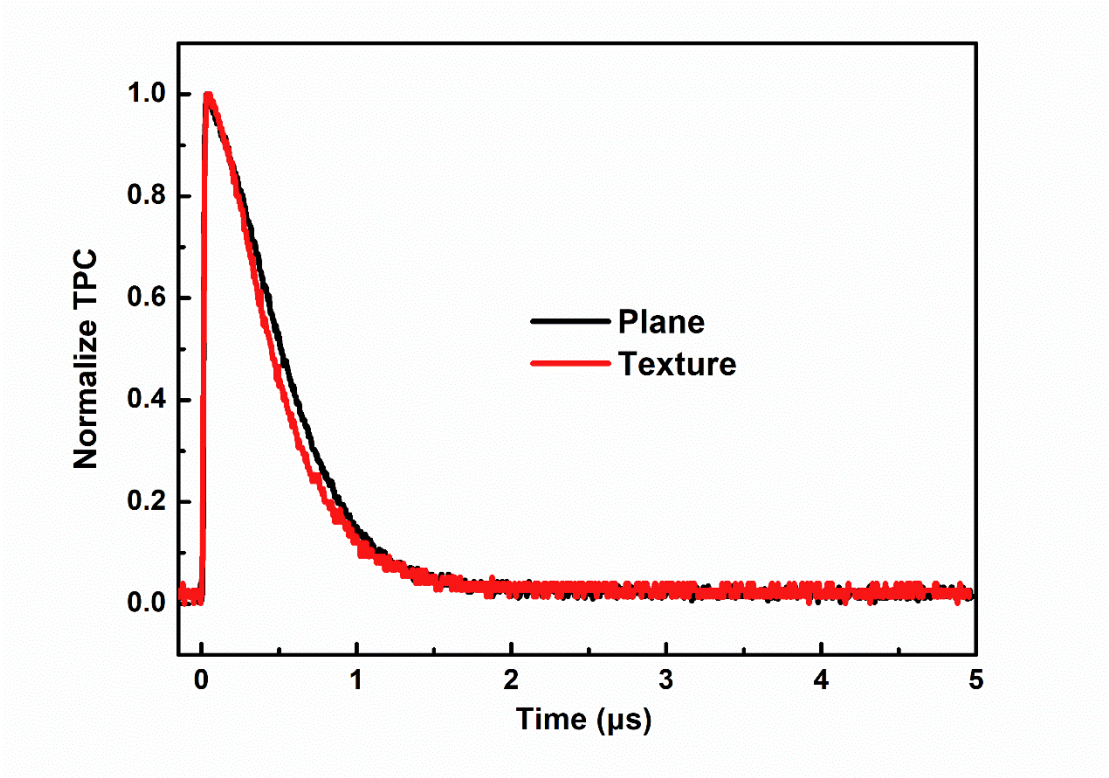

Figure S12. TPC measurements of devices with plane and optimized texture PTAA.

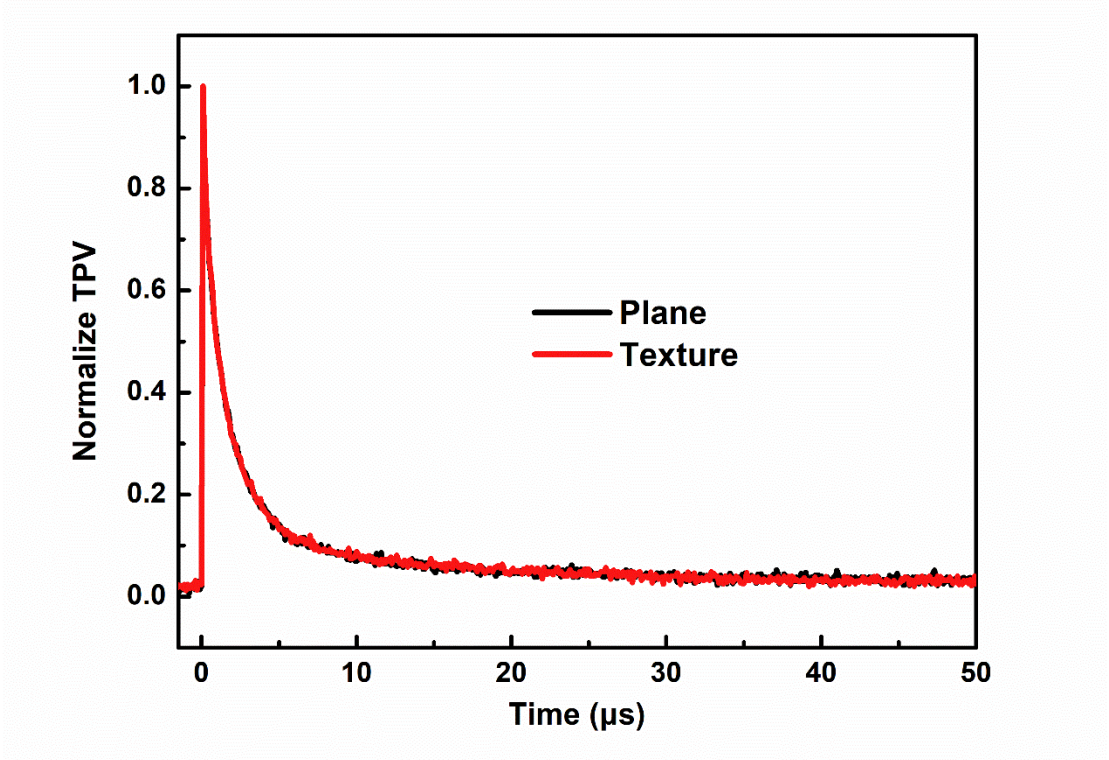

Figure S13. TPV measurements of devices with plane and optimized texture PTAA.

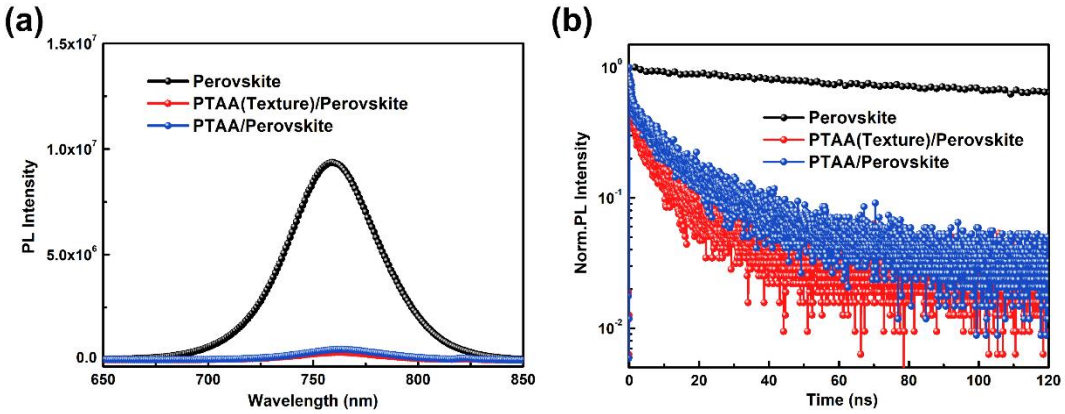

Figure S14. PL spectra for perovskite on glass (black), textured PTAA (red) and plane PTAA (blue) samples. (b) Normalized TRPL decay of the perovskite films on three different substrates.

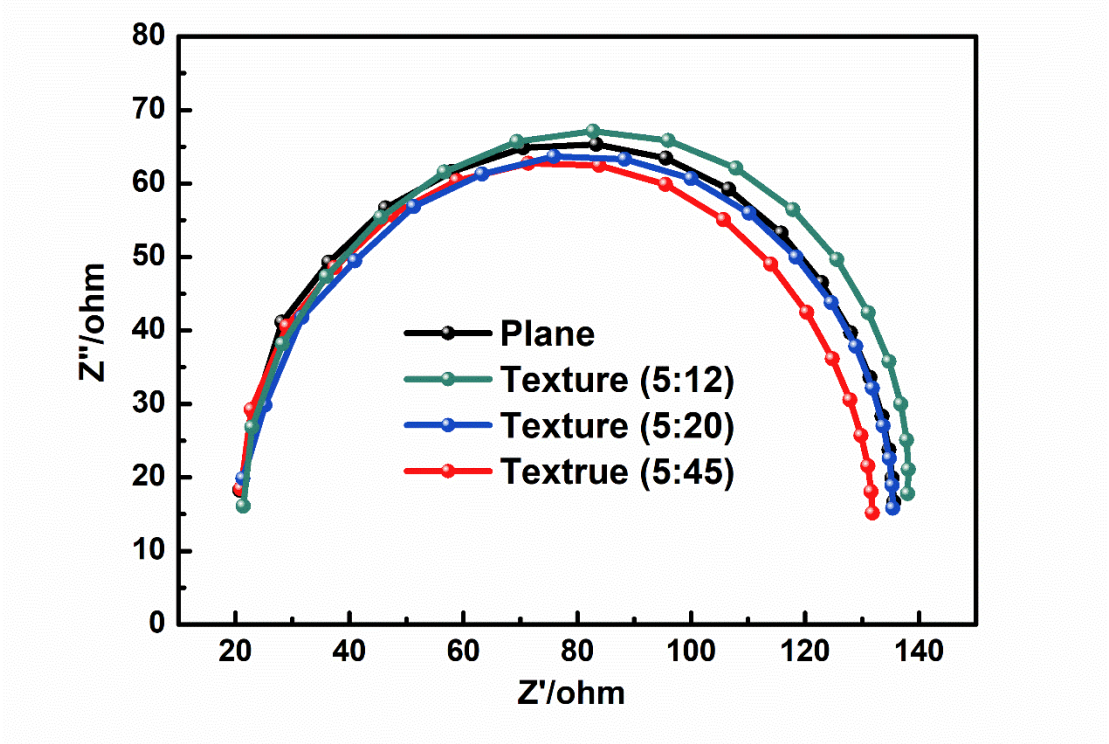

Figure S15. The Nyquist plots for samples with plane PTAA and different textured PTAA.

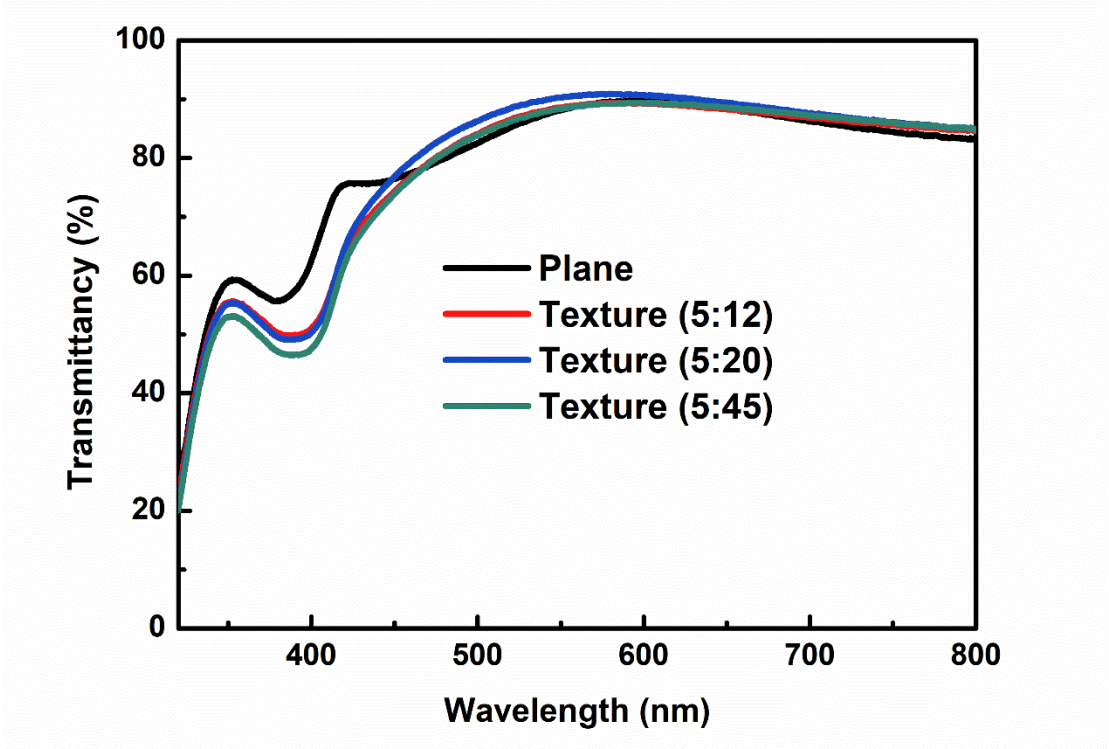

Figure S16. The transmittance of glass/ITO/PTAA with plane and different texture PTAA HTL layers.

TCO	HTL	Perovskite	ETL	PCE (%)	J_{SC} (mA • cm^{-2})	V_{OC} (V)	FF (%)	Time (year)	Ref.	DOI
ITO	P3CT-CH_3NH_2	$MAPbI_3$	PCBM/BCP	19.6	22.2	1.09	81	2018	1	10.1021/acsami.7b11977
ITO	P3CT-K	$MAPbI_3$	PCBM-GO/ZnO	20	24.1	1.05	79	2018	2	10.1016/j.nanoen.2018.02.014
ITO	P3CT-N	$MAPbI_3$	PCBM/BCP	20.9	22.8	1.1	83.2	2019	3	10.1039/c9ta04192c
ITO	P3CT-Na	$MAPbI_3$	TPE-PDI4/C60/BCP	18.8	21.9	1.05	81	2018	4	10.1039/c8ta06081a
ITO	P3CT-Na	$MAPbI_3$	ITCPTC/C60/BCP	19.5	22.1	1.07	82	2018	5	10.1039/c8ta06730a
ITO	P3CT-Na	$MAPbI_3$	IDT6CN-4F/BCP	19.8	22.3	1.07	83	2018	6	10.1039/c8ta10975c
ITO	P3CT-Na	$MAPbI_3$	ITCPTC-Th/BCP	18.8	22.5	1.06	78	2017	7	10.1039/c8ta00492g
ITO	PEDOT:PSS	$FA_{0.85}MA_{0.15}Pb\ (I_{0.85}Br_{0.15})_3$	C60/BCP	21	23.1	1.06	86	2018	8	10.1021/acsnano.8b05731
ITO	PEDOT:PSS	FAPbI3-xBrx	NDI-PM	20	23	1.06	79.8	2017	9	10.1039/c7ta06900f
ITO	PEDOT:PSS	$FAPbI_{3-x}Br_x$	NDI-ID	20.2	23	1.1	80	2018	10	10.1002/adfm.201800346
ITO	PEDOT:PSS	FAPbI3-xBrx	NDI-PhE	20.5	23.1	1.1	80.8	2018	11	10.1002/cssc.201802234
ITO	PEDOT:PSS	$MAPbI_3$	PCBM	18.9	21.4	1.11	79.6	2017	9	10.1039/c7ta06900f
ITO	PEDOT:PSS	$MAPbI_3$	PCBM/BCP	18.7	22.4	1.02	82	2016	12	10.1002/adma.201604048
FTO	PEDOT:PSS	$MAPbI_3$	HBM	20.6	22.4	1.12	82	2019	13	10.1021/acs.nanolett.9b00936
ITO	PEDOT:PSS	$MAPbI_{3-x}Cl_x$	INIC/PCBM/PDIN	19.3	23.1	1.01	82.7	2017	14	10.1039/c7ta06923e
ITO	PEDOT:PSS	$(FAPbI_3)_{0.8}(MAPbBr_3)_{0.2}$	PCBM/BCP	20.3	22.4	1.13	80	2018	15	10.1002/adma.201805554
ITO	PTAA(F_4-TCNQ)	$MAPbI_3$	PS/C60/BCP	19.4	22.3	1.16	75.2	2017	16	10.1002/adma.201700159
ITO	PTAA	$MAPbI_3$	PCBM/BCP	19.3	23.4	1.04	78.8	2018	17	10.1002/smll.201804692
ITO	PTAA(F_4-TCNQ)	$(FA_{0.95}PbI_{2.95})_{0.85}(MAPbBr_3)_{0.15}$	PCBM/BCP	20.9	21.9	1.18	81.4	2018	18	10.1126/science.aap9282
ITO	PTAA(F_4-TCNQ)	$MAPbI_3$	PCBM/BCP	19.0	22.5	1.1	76.8	2017	19	10.1002/adfm.201704836
ITO	PTAA(F_4-TCNQ)	$MAPbI_3$	PCBM/Bphen	20.2	23.4	1.12	77.6	2018	20	10.1002/smll.201704007
ITO	PTAA-Doped	$MA_{0.6}FA_{0.4}PbI_3$	PCBM/BCP	20.2	23.1	1.09	80	2017	21	10.1002/adma.201604758
ITO	TAPC(PTAA)	$MAPbI_{3-x}Cl_x$	C60/BCP	21.0	23.4	1.12	80.1	2018	22	10.1002/solr.201800173
ITO	PTAA(texture)	$MAPbI_{3-x}Cl_x$	PCBM/BCP	20.8	22.5	1.12	82.5	2019		this works

ITO	PTAA(AR-texture)	$MAPbI_{3-x}Cl_x$	PCBM/BCP	21.6	23.3	1.12	82.9	2019

Table S1. Literature survey of low temperature process HTL for p-i-n devices. The present study has been included for comparison.

Reference

(1) Li, X.; Wang, Y. C.; Zhu, L.; Zhang, W.; Wang, H. Q.; Fang, J. Improving Efficiency and Reproducibility of Perovskite Solar Cells Through Aggregation Control in Polyelectrolytes Hole Transport Layer, *ACS Appl. Mater. Inter.* **2017**, *9*, 31357-31361.

(2) Li, J.; Jiu, T.; Duan, C.; Wang, Y.; Zhang, H.; Jian, H.; Zhao, Y.; Wang, N.; Huang, C.; Li, Y. Improved Electron Transport in $MAPbI_3$ Perovskite Solar Cells Based on Dual Doping Graphdiyne, *Nano Energy* **2018**, *46*, 331-337.

(3) Wu, Y.; Wan, L.; Fu, S.; Zhang, W.; Li, X.; Fang, J. Liquid Metal Acetate Assisted Preparation of High-Efficiency and Stable Inverted Perovskite Solar Cells, *J. Mater. Chem. A* **2019**, *7*, 14136-14144.

(4) Jiang, K.; Wu, F.; Yu, H.; Yao, Y.; Zhang, G.; Zhu, L.; Yan, H. A Perylene Diimide-Based Electron Transport Layer Enabling Efficient Inverted Perovskite Solar Cells, *J. Mater. Chem. A* **2018**, *6*, 16868-16873.

(5) Zhu, L.; Gao, W.; Wu, F.; Li, L.; Yang, C.: Regulating the Electron Transporting Properties of Indacenodithiophene Derivatives for Perovskite Solar Cells with PCEs up to 19.51%, *J. Mater. Chem. A* **2018**, *6*, 18044-18049.

(6) Gao, W.; Wu, F.; Liu, T.; Zhang, G.; Chen, Z.; Zhong, C.; Zhu, L.; Liu, F.; Yan, H.; Yang, C. Multifunctional Asymmetrical Molecules for High-Performance Perovskite and Organic Solar Cells, *J. Mater. Chem. A* **2019**, *7*, 2412-2420.

(7) Wu, F.; Gao, W.; Yu, H.; Zhu, L.; Li, L.; Yang, C. Efficient Small-Molecule Non-Fullerene Electron Transporting Materials for High-Performance Inverted Perovskite Solar Cells, *J. Mater. Chem. A* **2018**, 6, 4443-4448.

(8) Chiang, C. H.; Wu, C. G. A Method for the Preparation of Highly Oriented $MAPbI_3$

Crystallites for High-Efficiency Perovskite Solar Cells to Achieve an 86% Fill Factor. *ACS Nano* **2018**, *12*, 10355-10364.

(9) Heo, J. H.; Lee, S.-C.; Jung, S.-K.; Kwon, O. P.; Im, S. H.: Efficient and Thermally Stable Inverted Perovskite Solar Cells by Introduction of Non-Fullerene Electron Transporting Materials, *J. Mater. Chem. A* **2017**, *5*, 20615-20622.

(10) Jung, S.-K.; Heo, J. H.; Lee, D. W.; Lee, S.-C.; Lee, S.-H.; Yoon, W.; Yun, H.; Im, S. H.; Kim, J. H.; Kwon, O. P. Nonfullerene Electron Transporting Material Based on Naphthalene Diimide Small Molecule for Highly Stable Perovskite Solar Cells with Efficiency Exceeding 20%, *Adv. Funct. Mater.* **2018**, *28*, 1800346.

(11) Jung, S. K.; Heo, J. H.; Lee, D. W.; Lee, S. H.; Lee, S. C.; Yoon, W.; Yun, H.; Kim, D.; Kim, J. H.; Im, S. H.; Kwon, O. P. Homochiral Asymmetric-Shaped Electron-Transporting Materials for Efficient Non-Fullerene Perovskite Solar Cells, *ChemSusChem* **2019**, *12*, 224-230.

(12) Chen, K.; Hu, Q.; Liu, T.; Zhao, L.; Luo, D.; Wu, J.; Zhang, Y.; Zhang, W.; Liu, F.; Russell, T. P.; Zhu, R.; Gong, Q. Charge-Carrier Balance for Highly Efficient Inverted Planar Heterojunction Perovskite Solar Cells, *Adv. Mater.* **2016**, *28*, 10718-10724.

(13) Yang, D.; Zhang, X.; Wang, K.; Wu, C.; Yang, R.; Hou, Y.; Jiang, Y.; Liu, S.; Priya, S. Stable Efficiency Exceeding 20.6% for Inverted Perovskite Solar Cells Through Polymer-Optimized PCBM Electron-Transport Layers, *Nano Lett*. **2019**, *19*, 3313-3320.

(14) Liu, K.; Dai, S.; Meng, F.; Shi, J.; Li, Y.; Wu, J.; Meng, Q.; Zhan, X. Fluorinated Fused Nonacyclic Interfacial Materials for Efficient and Stable Perovskite Solar Cells, *J. Mater. Chem. A* **2017**, *5*, 21414-21421.

(15) Wolff, C. M.; Zu, F.; Paulke, A.; Toro, L. P.; Koch, N.; Neher, D. Reduced

Interface-Mediated Recombination for High Open-Circuit Voltages in $CH_3NH_3PbI_3$ Solar Cells, *Adv. Mater.* **2017**, *29*, 1700159.

(16) Li, Z.; Liu, C.; Zhang, X.; Ren, G.; Han, W.; Guo, W. Developing 1D Sb-Embedded Carbon Nanorods to Improve Efficiency and Stability of Inverted Planar Perovskite Solar Cells, *Small* **2019**, *15*, e1804692.

(17) Luo, D.; Yang, W. Q.; Wang, Z. P.; Sadhanala, A.; Hu, Q.; Su, R.; Shivanna, R.; Trindade, G. F.; Watts, J. F.; Xu, Z. J.; Liu,T.H.; Chen, K.; Ye, F.J.; Wu, P.; Zhao, L.C.; Wu, J.; Tu, Y.G.; Zhang, Y.F.; Yang, X.Y.; Zhang, W.; *et al.* Enhanced Photovoltage for Inverted Planar Heterojunction Perovskite Solar Cells, *Science* **2018**, *360*, 1442–1446.

(18) Dong, H.; Wu, Z.; Xi, J.; Xu, X.; Zuo, L.; Lei, T.; Zhao, X.; Zhang, L.; Hou, X.; Jen, A. K. Y. Pseudohalide-Induced Recrystallization Engineering for $CH_3NH_3PbI_3$ Film and Its Application in Highly Efficient Inverted Planar Heterojunction Perovskite Solar Cells, *Adv. Funct. Mater.* **2018**, *28*, 1704836.

(19) Zhang, F.; Song, J.; Hu, R.; Xiang, Y.; He, J.; Hao, Y.; Lian, J.; Zhang, B.; Zeng, P.; Qu, J. Interfacial Passivation of the *p*-Doped Hole-Transporting Layer Using General Insulating Polymers for High-Performance Inverted Perovskite Solar Cells, *Small* **2018**, *14*, e1704007.

(20) Luo, D.; Zhao, L.; Wu, J.; Hu, Q.; Zhang, Y.; Xu, Z.; Liu, Y.; Liu, T.; Chen, K.; Yang, W.; Zhang, W.; Zhu, R.; Gong, Q. Dual-Source Precursor Approach for Highly Efficient Inverted Planar Heterojunction Perovskite Solar Cells, *Adv. Mater.* **2017**, *29*, 1604758.

(21) Yu, J. C.; Badgujar, S.; Jung, E. D.; Singh, V. K.; Kim, D. W.; Gierschner, J.; Lee, E.; Kim, Y. S.; Cho, S.; Kwon, M. S.; Song, M. H. Highly Efficient and Stable Inverted

Perovskite Solar Cell Obtained Via Treatment by Semiconducting Chemical Additive, *Adv. Mater.* **2019**, *31*, e1805554.

(22) Li, W.; Liu, C.; Li, Y.; Kong, W.; Wang, X.; Chen, H.; Xu, B.; Cheng, C. Polymer Assisted Small Molecule Hole Transport Layers Toward Highly Efficient Inverted Perovskite Solar Cells, *Solar RRL*, **2018**, *2*, 1800173.